DOI 10.1007/s11595-014-1051-z

Visible Light-induced Cr-doped $SrTiO_3$-g-C_3N_4 Composite for Improved Photocatalytic Performance

YANG Ming[1], JIN Xiaoqi[2]

(1.School of Transportation, Southeast University, Nanjing 210096, China; 2.Bio-Chemistry Department, Wenshan University, Wenshan 663000, China)

Abstract: Novel visible light-induced Cr-doped $SrTiO_3$-g-C_3N_4 composite photocatalysts were synthesized by introducing polymeric g-C_3N_4. The composite photocatalyst was characterized by X-ray diffraction (XRD), high-resolution transmission electron microscopy (HRTEM), Fourier transform infrared (FT-IR) spectroscopy, UV-vis diffuse reflection spectroscopy, photoluminescence (PL) spectroscopy and BET surface area measurements. The photocatalytic oxidation ability of the novel composite photocatalyst was evaluated using methyl orange (MO) as a target pollutant. The photocatalysts exhibited a significantly enhanced photocatalytic performance in degrading MO. The optimal g-C_3N_4 content for the photodegradation activity of the composite photocatalysts was determined. The as-prepared composite photocatalyst exhibits an improved photocatalytic activity due to enhancement of photo-generated electron-hole separation at the interface.

Key words: photocatalysis; g-C_3N_4; Cr-doped $SrTiO_3$; composite

1 Introduction

Photocatalysis has received considerable interest for application in removal of pollutant and in water splitting for hydrogen or oxygen generation by using solar energy. However, to realize the photocatalysis technique for large-scale industrial applications, highly efficient photocatalysts are still most important[1-2]. As one of the promising photocatalytic candidates, $SrTiO_3$ has attracted more and more attention due to its excellent photocatalytic performance[3]. However, due to the relatively large band gap (3.2 eV), $SrTiO_3$ only responds to the UV light. To decrease its band gap, doping of foreign elements into $SrTiO_3$ has been reported[4]. In particular, chromium (Cr) doping has attracted great interest because the occupied Cr^{3+} level is usually 1.0 eV higher than the valence band top formed by O 2p orbital or 2.2 eV lower than the conduction band bottom formed by Ti 3d orbital, which means that the band gap of $SrTiO_3$ can be narrowed and the visible light response can be achieved through the Cr doping[5,6].

To increase the separation efficiency of photogenerated electron-hole pairs is usually a good method to improve the photocatalytic activities, such as the use of co-catalysts[7]. Another feasible route is to form a composite photocatalyst between two kinds of semiconductors, and the suitably matching band level of conduction and valance bands can induce improved photocatalytic activity[8]. Polymer photocatalyst, graphitic carbon nitride (g-C_3N_4) which has been used for hydrogen or oxygen generation from water splitting under visible light irradiation has been reported by Wang *et al* for the first time[9]. Very recently, some composite photocatalysts, such as TiO_2-g-C_3N_4[10], C_3N_4-TaON[11], g-C_3N_4/Bi_2WO_6[12], graphene/C_3N_4[13,14], C_3N_4/$BiPO_4$[15], MWNTs/g-C_3N_4[16], g-C_3N_4-$SrTiO_3$:Rh[17], g-C_3N_4/ZnO[18], C_3N_4/$ZnWO_4$[19] and BiOBr-C_3N_4[20], have been prepared. To the best of our knowledge, there has been no report regarding the introduction of g-C_3N_4 to Cr-doped $SrTiO_3$ to enhance the photocatalytic activity.

In the present study, considering the synergic

(Received: Nov. 6, 2013; Accepted: Jan. 10, 2014)

YANG Ming(杨明): Assoc. Prof.; Ph D; E-mail:bartty_ym@sina.com

Funded by the National Natural Science Foundation of China (No. 51208102)

effect between Cr-doped $SrTiO_3$ and polymeric g-C_3N_4, the novel heterostructured Cr-doped $SrTiO_3$-g-C_3N_4 was prepared for the first time as a photocatalyst via mixing and heating methods. The characteristics of the organic-inorganic heterogeneous composite powders with various amounts of g-C_3N_4 were analyzed. The amount of g-C_3N_4 was optimized in terms of maximizing the photocatalytic activity for enhancing the MO photodegradation activity under visible light irradiation. The results demonstrated that compared with pure Cr-doped $SrTiO_3$ and g-C_3N_4, the Cr-doped $SrTiO_3$-g-C_3N_4 heterojunction photocatalyst had an improved MO photodegradation activity, and the possible photodegradation mechanism was also discussed.

2 Experimental

2.1 Materials

The starting materials utilized were $Sr(NO_3)_2$, $Cr(NO_3)_3$•$9H_2O$, $Ti(C_4H_9O)_4$, NaOH and ethylene glycol (EG) and melamine ($C_3H_6N_6$) (analysis purity grade, Sinopharm Chemical Reagent Co. Ltd.).

2.2 Synthesis of Cr-doped $SrTiO_3$–g-C_3N_4 composite

The Cr-doped $SrTiO_3$ was prepared by a sol-gel hydrothermal route[6]. In a typical process, $Sr(NO_3)_2$, $Cr(NO_3)_3$•$9H_2O$ and $Ti(C_4H_9O)_4$ were weighed out according to the stoichiometry of $Sr_{0.95}Cr_{0.05}TiO_3$. $Sr(NO_3)_2$ and $Cr(NO_3)_3$•$9H_2O$ were dissolved in EG and the solution was stirred at 80 ℃. Then $Ti(C_4H_9O)_4$ was dropped into the solution and a gel was prepared with the evaporation of EG. Then 5 mol·L^{-1} NaOH solution (30 mL) was added to the gel. After stirred for a certain time, it was transferred into a Teflon-lined stainless steel autoclave and heated at 200 ℃ for 24 h. The product was washed with distilled water until the pH value was 7-8 and dried at 80 ℃ for 12 h. The g-C_3N_4 photocatalyst was prepared by directly heating melamine at 500 ℃ (heating rate: 20 ℃·min^{-1}) for 2 h, and further deammonation treatment was set at 520 ℃ for 2 h[21] in the semiclosed system to prevent sublimation of melamine. Then, the mixture of Cr-doped $SrTiO_3$ and g-C_3N_4 powder was ground together with 20wt%, 40wt%, 60wt%, and 80wt% g-C_3N_4 (denoted as 20wt%, 40wt%, 60wt%, and 80wt% Cr-doped $SrTiO_3$-g-C_3N_4, respectively). Then, the mixture was calcined at 300 ℃ for 1 h in a tubular furnace under N_2 atmosphere. A mechanical mixed g-C_3N_4 and Cr-doped $SrTiO_3$ with 60wt% g-C_3N_4 and no heat treatment was also prepared as a reference (denoted as 60% Cr-doped $SrTiO_3$/g-C_3N_4).

2.3 Characterization

The products were characterized by X-ray diffraction (XRD) for phase identification on a Rigaku Ultima III diffractometer with Cu Kα radiation (λ = 0.154 nm, 40 kV, 40 mA) and a scan rate of 10 °•min^{-1}. The specific surface area of the as-prepared powders was obtained on a Micromeritics TriStar 3000 instrument (USA) at 77 K and Brunauer-Emmett-Teller (BET) equation was used to calculate the specific surface area. The infrared optical properties were measured on NEXUS870 IR spectrometer using KBr pellet technique. Ultraviolet visible (UV-vis) diffuse reflection spectra were recorded using a UV-vis spectrophotometer (Shimadzu UV-2550, Japan) and converted from reflection to absorbance by the Kubelka-Munk method. Their band gaps are calculated by the equation of $\alpha h\nu = A(h\nu - E_g)^{n/2}$, in which α, ν, A, and E_g signify the absorption coefficient, light frequency, proportionality constant, and band gap, respectively, and n equals 1 or 4, depending on whether the transition is direct or indirect, respectively. Here n = 1 because these materials are direct-gap semiconductors. The microstructure of the sample was observed by a high resolution transmission electron microscope (HR-TEM; JEM-2100, 200 kV, JEOL Ltd.). The acquired photoluminescence (PL) properties of the as-prepared composite catalysts were detected with a spectrofluorometer (VARIAN, Cary Eclipse, USA) at room temperature.

2.4 Photocatalytic activity tests

The methyl orange (MO) dye was used to test the photocatalytic activities of samples. The photocatalytic reaction was preformed in a Pyrex reactor. The catalyst (0.1 g) was dispersed in MO aqueous solution (100 mL, 4.2 mg·L^{-1}). The light irradiation system contains a 300 W Xe lamp with cut-off filter L42 for visible light and a water filter to remove heating effects. The reaction solutions for all experiments of the MO photodegradation were first stirred in the dark for 1 h to reach the adsorption-desorption equilibrium of MO on catalysts. The degradation efficiency of MO was evaluated using the UV-vis absorption spectra to measure the peak value of a maximum absorption of MO solution at the wavelength of 463 nm.

3 Results and discussion

The powder XRD patterns of g-C_3N_4, Cr-doped

$SrTiO_3$ and Cr-doped $SrTiO_3$-g-C_3N_4 composite are shown in Fig.1. It can be seen that there are two peaks found in sample with 100% g-C_3N_4 at 27.40°and 13.08°, which can be indexed to (002) peak (the characteristic inter-layer staking peak of aromatic systems) and (100) diffraction planes (the in-plane structural packing motif) of the graphite-like carbon nitride[21] respectively. The XRD pattern (Fig.1) indicates that the Cr-doped $SrTiO_3$ sample is very similar to the cubic $SrTiO_3$, and all Bragg diffraction peaks which can be indexed as (110), (111), (200), (211), (220) and (310) are in good agreement with JPCDS No. 89-4934. The inset of Fig.1 shows a magnified image of the diffraction peaks for the (110) plane. The peak is shifted toward a higher angle by the doping of Cr ions, which confirmed the incorporation of the Cr ions into the $SrTiO_3$ crystal lattice due to the smaller ionic radius of the Cr^{3+} (0.0615 nm) than that of Sr^{2+} (0.118 nm)[6]. The Cr-doped $SrTiO_3$-g-C_3N_4 composite samples present two components: g-C_3N_4 and Cr-doped $SrTiO_3$-g-C_3N_4, and the intensity of the (002) peak of g-C_3N_4 becomes stronger with the increase of the content of g-C_3N_4.

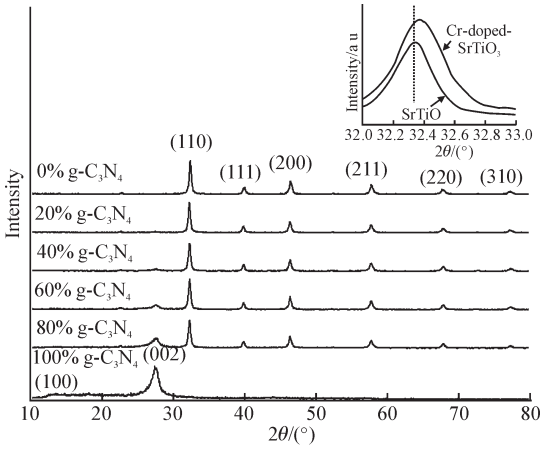

Fig.1 XRD patterns of the Cr-doped $SrTiO_3$ and g-C_3N_4 composite with different proportions. Inset shows diffraction peak positions of the (110) plane in the range of 2θ = 32-33°

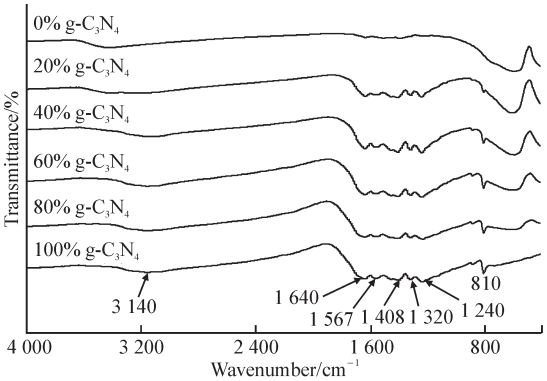

Fig.2 FTIR spectra of the Cr-doped $SrTiO_3$ and g-C_3N_4 composite with different proportions

Fig.2 shows the Fourier transform infrared (FT-IR) spectra of g-C_3N_4, Cr-doped $SrTiO_3$ and Cr-doped $SrTiO_3$-g-C_3N_4 composite respectively. The FT-IR spectra of the as-prepared g-C_3N_4 show the features very similar to those of the published results[10]. The absorption band near 1640 cm^{-1} is attributed to C-N stretching, while the other three absorption bands near 1 240, 1 320 and 1 408 cm^{-1} are attributed to aromatic C-N stretching. A broad band near 3140 cm^{-1} corresponds to the stretching modes of terminal NH_2 or NH groups at the defect sites of the aromatic ring[10]. The band near 810 cm^{-1} is attributed to out-of plane bending modes of C-N heterocycles. The FT-IR spectra of Cr-doped $SrTiO_3$-g-C_3N_4 composites show that the characteristic bands for g-C_3N_4 still remain. For the pure Cr-doped $SrTiO_3$, the broad absorption in the range of 500-800 cm^{-1} may be attributed to TiO_6 octahedron stretching vibration[22], while for the composite, with the increase of the content of g-C_3N_4, the intensity of the broad band decreases maybe due to the existence of the organic component.

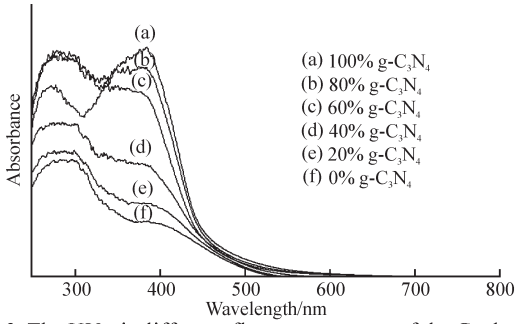

Fig.3 The UV-vis diffuse reflectance spectra of the Cr-doped $SrTiO_3$ and g-C_3N_4 composite with different proportions

UV-vis diffuse reflectance spectroscopy was used to investigate the optical properties of the samples. Fig.3 shows the UV-vis absorption spectra of g-C_3N_4, Cr-doped $SrTiO_3$ and Cr-doped $SrTiO_3$-g-C_3N_4 composite. The absorption edge of the Cr-doped $SrTiO_3$ sample occurs at ca. 540 nm, and the band gap energy is calculated as 2.30 eV.

After coupled with g-C_3N_4, the absorption edge shifts to the higher energy region. It can be seen that the absorption edges of the composite samples shift remarkably to shorter wavelengths with increasing amount of g-C_3N_4. The increase in band gaps of the samples is from 2.30 eV of Cr-doped $SrTiO_3$ to 2.70 eV of g-C_3N_4 when the content of g-C_3N_4 is increased from 0% to 100%. The morphology of 60wt% Cr-doped $SrTiO_3$-g-C_3N_4 composite material is investigated using TEM and high-resolution TEM (HRTEM), as shown in Figs.4(a) and 4(b) respectively. The particle size of

the Cr-doped $SrTiO_3$ is estimated to be in the range of approximately 20-30 nm. The HRTEM image (Fig.4(b)) shows that the lattice fringes have a spacing of 0.27 nm corresponding to interplanar spacing of (110) plane of Cr-doped $SrTiO_3$. This observation is consistent with the XRD result.

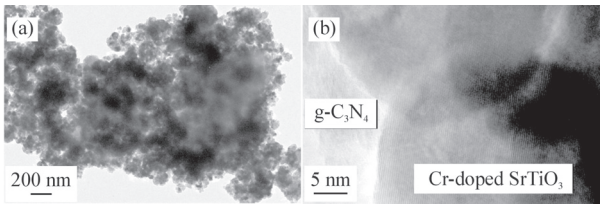

Fig.4 TEM (a) and HRTEM (b) images of 60wt% Cr-doped $SrTiO_3$-g-C_3N_4 composite

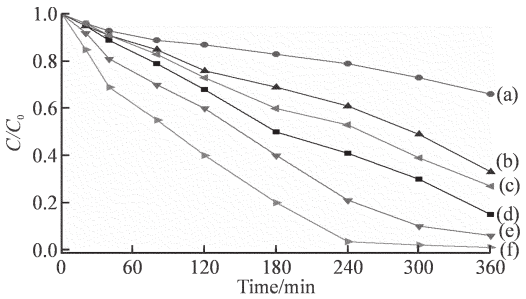

Fig.5 MO photodegradation over the Cr-doped $SrTiO_3$ and g-C_3N_4 composite with different g-C_3N_4 proportions: (a) 0%; (b) 20%; (c) 40%; (d) 100%; (e) 80% and (f) 60%

The activities for MO photodegradation over the investigated samples are shown in Fig.5. In our experiments, MO photolysis under visible light irradiation in the absence of catalyst is not observable. This indicates that MO is stable under visible light irradiation. From Fig.5, it can be seen that, after 360 min of visible light illumination, MO removal over Cr-doped $SrTiO_3$ is as low as 44% and that g-C_3N_4 shows a photocatalytic performance with a degradation ratio of 85%. The as-prepared composite photocatalysts with 60wt% or 80wt% g-C_3N_4 show better activity than single-phase g-C_3N_4 or Cr-doped $SrTiO_3$. Significantly, the 60wt% Cr-doped $SrTiO_3$-g-C_3N_4 presents a sharp increase in the catalytic activity for MO decomposition, which induced 100% degradation within 240 min light irradiation. 8.9%, 12.9%, 12.4%, 13.8%, and 12.6% MO before the photoreaction was adsorbed on the surface of g-C_3N_4, Cr-doped $SrTiO_3$ and 20%, 40%, 60%, 80% Cr-doped $SrTiO_3$-g-C_3N_4, respectively. After 240 min light irradiation, 59.1%, 21.2%, 39.0%, 47.3%, 100%, 79.5% MO was photocatalytically degraded over g-C_3N_4, Cr-doped $SrTiO_3$ and 20%, 40%, 60%, 80% Cr-doped $SrTiO_3$-g-C_3N_4, respectively (see Fig.5). For the Cr-doped $SrTiO_3$-g-C_3N_4 composite, the g-C_3N_4 content was important to achieve the high photocatalytic activity. The suitable content of g-C_3N_4 caused its well dispersion on the Cr-doped $SrTiO_3$ surface, which promoted the transfer and separation of photogenerated electrons and holes. However, at contents higher than 60wt%, the heterojunction structures and interfaces between the g-C_3N_4 and Cr-doped $SrTiO_3$ particles decreased. The interfacial charge transfer was suppressed and thus the photocatalytic activity was reduced. Therefore, the 60wt% Cr-doped $SrTiO_3$-g-C_3N_4 was the best performing sample and was selected for the cycling tests.

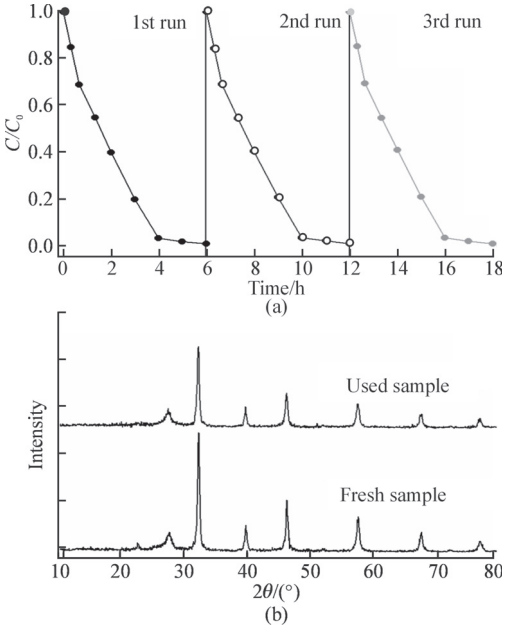

Fig.6 Stability test for the 60wt% Cr-doped $SrTiO_3$-g-C_3N_4 photocatalysis system: (a) cycling runs for photodegradation of MO under visible light irradiation; (b) XRD patterns for 60wt% Cr-doped $SrTiO_3$-g-C_3N_4 composite before and after the cycling photocatalytic reaction

The stability of a photocatalyst is a crucial factor for its application and assessment. The cycling reactions for three times for the photodegradation of MO over the 60wt% Cr-doped $SrTiO_3$-g-C_3N_4 photocatalyst were performed to evaluate its photocatalytic stability and the results are shown in Fig.6. The separated photocatalyst was washed with deionized water and dried after every 6 h of photodegradation. Fig.6(a) shows that a high MO photodegradation could be maintained after 3 cycling runs and there was no obvious catalyst deactivation. The XRD patterns (Fig.6(b)) also show that the crystal structure of the Cr-doped $SrTiO_3$-g-C_3N_4 photocatalysts did not change after the photocatalytic reaction. These evidences indicate that the Cr-doped $SrTiO_3$-g-C_3N_4 photocatalyst can be concluded as stable.

For comparison, the commercial nitrogen-doped-TiO_2 with a specific surface area about

65 $m^2 \cdot g^{-1}$ (TPS201, Sumitomo Corp. Japan) and the mixed material of g-C_3N_4 and Cr-doped $SrTiO_3$ without heat treatment (60wt% Cr-doped $SrTiO_3$/g-C_3N_4) were also used as photocatalysts in degradation of MO. Fig.7 shows the degradation activities of MO over different photocatalysts under visible light irradiation. As shown in Fig.7, the 60% Cr-doped $SrTiO_3$-g-C_3N_4 composite show much higher activity than that of nitrogen-doped TiO_2 and 60wt% Cr-doped $SrTiO_3$/g-C_3N_4 photocatalysts. This clearly indicates that the advantage of heating treatment is the formation of chemically bonded interfaces between the two materials, and the Cr-doped $SrTiO_3$-g-C_3N_4 was determined as an efficient visible light photocatalyst for the degradation of MO.

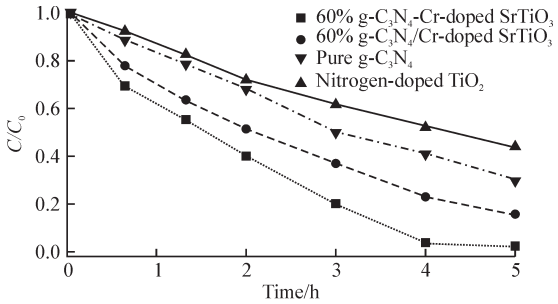

Fig.7 Comparison of MO degradation over different photocatalysts under visible light irradiation

In general, hydroxyl radicals ($^{\bullet}OH$) and superoxide ($O_2^{\bullet}$ or $HOO^{\bullet}$) reactive oxidation species, are formed during the photocatalytic reaction[23]. Hydroxyl radical may be the active species for composite system[24]. $^{\bullet}OH$ is generated via the photogenerated hole oxidation[25] or multistep reduction of O_2 induced by photogenerated electron ($O_2 + e \rightarrow O_2^{\bullet-}$, $O_2^{\bullet-} + e + 2H^+ \rightarrow H_2O_2$, $H_2O_2 + e \rightarrow {}^{\bullet}OH + OH^-$)[26]. The photodegradation activity of photocatalysts is generally associated with the oxidation ability of photogenerated holes in valence band and reduction ability of photogenerated electrons in conduction band[23]. The oxidation potential of g-C_3N_4 is 1.57 V[12], which means that the photogenerated holes are incapable of directly oxidizing adsorbed hydroxyl groups to generate hydroxyl radicals (2.7 V *vs* NHE)[23]. Therefore, a reliable speculation may be that the $^{\bullet}OH$ in the composite photocatalysis system is formed from the multistep reduction of O_2 under light irradiation.

The BET specific surface area of the g-C_3N_4, Cr-doped $SrTiO_3$, 20wt%, 40wt%, 60wt%, and 80wt% Cr-doped $SrTiO_3$-g-C_3N_4 sample is 8.20, 23.10, 20.10, 18.20, 16.01, and 14.40 $m^2 \cdot g^{-1}$, respectively. Thus, the improved photocatalytic activity is not attributed to the effect of the specific surface area. The enhancement of photocatalytic performance of the composite materials

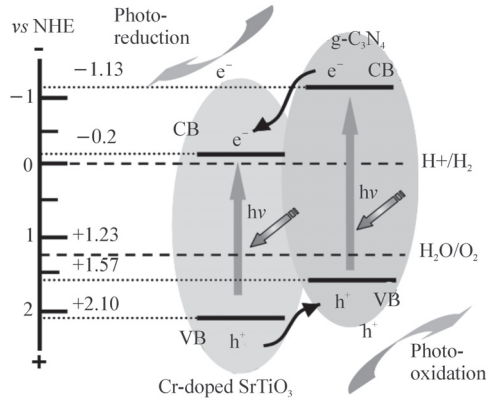

Fig.8 The schematic illustration for the electron-hole separation and transport at the visible light-driven g-C_3N_4-Cr-doped $SrTiO_3$ composite photocatalyst interface

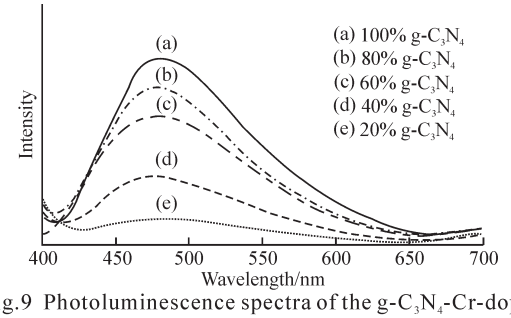

Fig.9 Photoluminescence spectra of the g-C_3N_4-Cr-doped $SrTiO_3$ composite photocatalysts

is supposed to be attributed to the more effective separation of the photogenerated electron-hole pairs. Based on the band gap positions, the CB and VB edge potentials of polymeric g-C_3N_4 were determined as −1.13 and +1.57 eV at pH 7 (versus the normal hydrogen electrode)[12], respectively. The conduction band level of $SrTiO_3$ is −0.2 eV[27]. Therefore, the occupied Cr^{3+} level in Cr-doped $SrTiO_3$ is estimated to be 2.1 eV according to the band gap of 2.3 eV which was determined from the UV-Vis absorption spectra (Fig. 3). Since the CB edge potential of g-C_3N_4 (−1.13 eV) is more negative than that of Cr-doped $SrTiO_3$ (−0.2 eV), the photo-induced electrons on g-C_3N_4 particle surfaces transfer more easily to Cr-doped $SrTiO_3$ via the well developed interface. Similarly, the photo-induced holes on the Cr-doped $SrTiO_3$ surface move to g-C_3N_4 due to the large difference in VB edge potentials. The scheme for electron-hole separation and transport at the visible-light-driven organic-inorganic composite photo catalyst interface is shown in Fig.8. This reduces the probability of electron-hole recombination and leads to a larger amount of electrons on the Cr-doped $SrTiO_3$ surface and holes on the g-C_3N_4 surface, respectively, which promotes the photocatalytic reactions to decompose MO.

PL analysis has been used to investigate the

migration and recombination processes of photo-generated electrons and holes in semiconductors[12,13]. To further confirm the above-proposed mechanism, the PL spectra of the Cr-doped $SrTiO_3$-g-C_3N_4 composite photocatalysts at an excitation wavelength of 330 nm are investigated and shown in Fig.9. The emission band for pure g-C_3N_4 is centered at 478 nm, which is attributed to the radiative recombination process of self-trapped excitations[12]. The positions of the Cr-doped $SrTiO_3$-g-C_3N_4 emission peaks are similar to that of pure g-C_3N_4. Obviously, compared with pure g-C_3N_4, the emission intensity of the Cr-doped $SrTiO_3$-g-C_3N_4 composite samples is much lower. The PL results indicate that the recombination of photogenerated electrons and holes was inhibited in the composite semi-conductors, which conforms to the discussion about the separation of charge carriers and photocatalytic experiments.

4 Conclusions

In summary, we have fabricated a Cr-doped $SrTiO_3$-g-C_3N_4 composite photocatalyst by introducing polymeric g-C_3N_4 via a mixing and heating method. The stable dye MO was selected as a substrate to evaluate the photocatalytic activity of Cr-doped $SrTiO_3$-g-C_3N_4. Our results clearly indicate that the visible-light-driven Cr-doped $SrTiO_3$-g-C_3N_4 heterojunction has a good performance in photo-oxidation of this organic pollutant, which resulted from the suitably matching conduction and valance band levels that improved the separation efficiency of photogenerated electron-hole pairs.

References

[1] Tank CM, Sakhare YS, Kanhe NS, *et al.* Electric Field Enhanced Photocatalytic Properties of TiO_2 Nanoparticles Immobilized in Porous Silicon Template[J]. *Solid State Sci*., 2011, 13: 1 500-1 504

[2] Dholam R, Patel N, Adami M, *et al*. Hydrogen Production by Photocatalytic Water-Splitting Using Cr- or Fe-Doped TiO_2 Composite Thin Films Photocatalyst[J]. *Int. J. Hydrogen Energy*, 2009, 34: 5 337-5 346

[3] Domen K, Kudo A, Onishi T. Photocatalytic Decomposition of Water into Hydrogen and Oxygen over Nickel(II) Oxide-Strontium Titanate (SrTiO3) Powder. 1. Structure of the Catalysts[J]. *J. Phys. Chem*., 1986, 90: 292-295

[4] Wang JS, Yin S, Komatsu M, *et al*. Preparation and Characterization of Nitrogen Doped $SrTiO_3$ Photocatalyst[J]. *J. Photochem. Photobiol., A*, 2004, 165:149; Konta R, Ishii T, Kudo A, Photocatalytic Activities of Noble Metal Ion Doped $SrTiO_3$ under Visible Light Irradiation[J]. *J. Phys. Chem. B*, 2004, 108: 8 992; Wei W, Dai Y, Guo M, *et al.* Density Functional Characterization of the Electronic Structure and Optical Properties of N-Doped, La-Doped, and N/La-Codoped $SrTiO_3$[J]. *J. Phys. Chem. C*, 2009, 113: 15 046-15 050

[5] Umebayashi T, Yamaki T, Itoh H, *et al.* Analysis of Electronic Structures of 3d Transition Metal-Doped TiO_2 Based on Band Calculations[J]. *J. Phys. Chem. Solids*, 2002, 63: 1 909 -1 920

[6] Yu H, Ouyang SX, Yan SC, *et al.* Sol-Gel Hydrothermal Synthesis of Visible- Light-Driven Cr-Doped $SrTiO_3$ for Efficient Hydrogen Production[J]. *J. Mater. Chem*., 2011, 21: 11 347-11 351

[7] Osterloh FE, Inorganic Materials as Catalysts for Photochemical Splitting of Water[J]. *Chem. Mater*., 2008, 20: 35-54

[8] Lin XP, Xing JC, Wang WD, *et al*. Photocatalytic Activities of Heterojunction Semiconductors Bi_2O_3/$BaTiO_3$: A Strategy for the Design of Efficient Combined Photocatalysts[J]. *J. Phys. Chem. C*, 2007, 111: 18 288-18 293

[9] Wang XC, Maeda K, Thomas A, *et al*. A Metal-Free Polymeric Photocatalyst for Hydrogen Production from Water under Visible Light[J]. *Nat. Mater*., 2009, 8: 76-80

[10] Yan HJ, Yang HX, TiO_2–g-C_3N_4 Composite Materials for Photocatalytic H_2 Evolution under Visible Light Irradiation[J]. *J. Alloys Compd*., 2011, 509: L26 -L29

[11] Yan SC, Lv SB, Li ZS, *et al*. Organic-Inorganic Composite Photo- catalyst of g-C_3N_4 and TaON with Improved Visible Light Photocatalytic Activities[J]. *Dalton Trans*., 2010, 39: 1 488- 1491

[12] Ge L, Han CC, Liu J. Novel Visible Light-Induced g-C_3N_4/Bi_2WO_6 Composite Photocatalysts for Efficient Degradation of Methyl Orange[J]. *Appl. Catal. B: Environ*., 2011, 108-109: 100-107

[13] Xiang QJ, Yu JG, Jaroniec M, Preparation and Enhanced Visible-Light Photo- catalytic H2-Production Activity of Graphene/C_3N_4 Composites[J]. *J. Phys. Chem. C*, 2011, 115: 7 355-7 363

[14] Li XH, Chen JS, Wang XC, *et al*. Metal-Free Activation of Dioxygen by Graphene/g-C_3N_4 Nanocomposites: Func- tional Dyads for Selective Oxidation of Saturated Hydrocarbons[J]. *J. Am. Chem. Soc*., 2011, 133: 8 074-8 077

[15] Pan CS, Xu J, Wang YJ, *et al*. Dramatic Activity of C_3N_4/$BiPO_4$ Photocatalyst with Core/Shell Structure Formed by Self-Assembly[J]. *Adv. Funct. Mater*., 2012, 22: 1 518-1 524

[16] Ge L, Han CC, Synthesis of MWNTs/g-C_3N_4 Composite Photo- catalysts with Efficient Visible Light Photocatalytic Hydrogen Evolution Activity[J]. *Appl. Catal. B: Environ*., 2012, 117-118: 268-274

[17] Kang HW, Lim SN, Song DS, *et al*. Organic-Inorganic Composite of g-C_3N_4–$SrTiO_3$: Rh Photocatalyst for Improved H_2 Evolution under Visible Light Irradiation[J]. *Inter. J. Hydro. Energy*, 2012, 37: 11 602-11 610

[18] Liu W, Wang ML, Xu CX, *et al*. Facile Synthesis of g-C_3N_4/ZnO Composite with Enhanced Visible Light Photooxidation and Photoreduction Properties[J]. *Chem. Engineering J*., 2012, 209: 386-393

[19] Wang YJ, Wang ZX, Muhammad S, *et al.* Graphite-Like C_3N_4 Hybri-dized $ZnWO_4$ Nanorods: Synthesis and Its Enhanced Photocatalysis in Visible Light[J]. *CrystEngComm*, 2012, 14: 5 065-5 070

[20] Fu J, Tian YL, Chang BB, *et al*. BiOBr-Carbon Nitride Heterojunc-tions: Synthesis, Enhanced Activity and Photocatalytic Mechanism[J]. *J. Mater. Chem*., 2012, 22: 21 159-21 166

[21] Yan SC, Li ZS, Zou ZG, Photodegradation Performance of g-C_3N_4 Fabricated by Directly Heating Melamine[J]. *Langmuir*, 2009, 25: 10 397-10 401

[22] Tan S, Yue S, Zhang Y, Jahn-Teller Distortion Induced by Mg/Zn Substitution On Mn Sites In The Perovskite Manganites[J]. *Physics Letters A*, 2003, 319: 530; Liu JW, Chen G, Li ZH, *et al.* Electronic Structure and Visible Light Photocatalysis Water Splitting Property of Chromium-Doped $SrTiO_3$[J]. *J. Solid State Chem*., 2006, 179: 3 704-3 708

[23] Yan SC, Li ZS, Zou ZG. Photodegradation of Rhodamine B and Methyl Orange over Boron-Doped g-C_3N_4 under Visible Light Irradiation[J]. *Langmuir*, 2010, 26: 3 894-3 901

[24] Yang M, Huang Q, Jin XQ. ZnGaNO Solid Solution-C_3N_4 Composite for Improved Visible Light Photocatalytic Performance[J]. *Materials Science and Engineering B*, 2012, 177: 600-605

[25] Yoon SH, Lee JH, Oxidation Mechanism of As(III) in the UV/TiO_2 System: Evidence for a Direct Hole Oxidation Mechanism[J]. *Environ. Sci. Technol*., 2005, 39: 9 695-9 701

[26] Liu GG, Li XZ, Zhao JC, *et al.* Photooxidation Mechanism of Dye Alizarin Red in TiO_2 Dispersions under Visible Illumination: An Experimental and Theoretical Examination[J]. *J. Mol. Catal. A: Chem*., 2000, 153: 221-229

[27] Kato H, Kudo A, Visible-Light-Response and Photocatalytic Activities of TiO_2 and $SrTiO_3$ Photocatalysts Codoped with Antimony and Chromium[J]. *J. Phys. Chem. B*, 2002, 106: 5 029 -5 034